



This is a repository copy of *3D-printed membrane for guided tissue regeneration* .

White Rose Research Online URL for this paper:  
<http://eprints.whiterose.ac.uk/125308/>

Version: Accepted Version

---

**Article:**

Tayebi, L., Rasoulianboroujeni, M., Moharamzadeh, K. et al. (3 more authors) (2018)  
3D-printed membrane for guided tissue regeneration. *Materials Science and Engineering: C*, 84. pp. 148-158. ISSN 0928-4931

<https://doi.org/10.1016/j.msec.2017.11.027>

---

Article available under the terms of the CC-BY-NC-ND licence  
(<https://creativecommons.org/licenses/by-nc-nd/4.0/>)

**Reuse**

This article is distributed under the terms of the Creative Commons Attribution-NonCommercial-NoDerivs (CC BY-NC-ND) licence. This licence only allows you to download this work and share it with others as long as you credit the authors, but you can't change the article in any way or use it commercially. More information and the full terms of the licence here: <https://creativecommons.org/licenses/>

**Takedown**

If you consider content in White Rose Research Online to be in breach of UK law, please notify us by emailing [eprints@whiterose.ac.uk](mailto:eprints@whiterose.ac.uk) including the URL of the record and the reason for the withdrawal request.



[eprints@whiterose.ac.uk](mailto:eprints@whiterose.ac.uk)  
<https://eprints.whiterose.ac.uk/>

## 3D-PRINTED **MEMBRANE** FOR GUIDED TISSUE REGENERATION

Lobat Tayebi<sup>1,2</sup>, Morteza Rasoulianboroujeni<sup>2</sup>, Keyvan Moharamzadeh<sup>3</sup>, Thafar KD Almela<sup>3</sup>, Zhanfeng Cui<sup>1</sup>, Hua Ye,<sup>1,\*</sup>

<sup>1</sup>Institute of Biomedical Engineering, Department of Engineering Science, University of Oxford, Oxford OX3 7DQ, UK

<sup>2</sup>Marquette University School of Dentistry, Milwaukee, WI, 53233, US

<sup>3</sup>School of Clinical Dentistry, University of Sheffield, Sheffield, S10 2TA, UK

\*Corresponding Author: Email: hua.ye@eng.ox.ac.uk, Phone +44 (0)1865 617689

### **Abstract:**

Three-dimensional (3D) printing is currently being intensely studied for a diverse set of applications, including the development of bioengineered tissues, as well as the production of functional biomedical materials and devices for dental and orthopedic applications. The aim of this study was to develop and characterize a 3D-printed hybrid construct that can be potentially suitable for guided tissue regeneration (GTR). For this purpose, the rheology analyses have been performed on different bioinks and a specific solution comprising 8% gelatin, 2% elastin and 0.5% sodium hyaluronate has been selected as the most suitable composition for printing a structured membrane for GTR application. Each membrane is composed of 6 layers with strand angles from the first layer to the last layer of 45, 135, 0, 90, 0 and 90°. Confirmed by 3D Laser Measuring imaging, the membrane has small pores on one side and large pores on the other to be able to accommodate different cells like osteoblasts, fibroblasts and keratinocytes on different sides. The ultimate cross-linked product is a 150 µm thick flexible and bendable membrane with easy surgical handling. Static and dynamic mechanical testing revealed static tensile modules of  $1.95 \pm 0.55$  MPa and a dynamic tensile storage modulus of  $314 \pm 50$  kPa. Through seeding the membranes with fibroblast and keratinocyte cells, the results of in vitro tests, including histological analysis, tissue viability examinations and DAPI staining, indicated that the membrane has desirable in vitro biocompatibility. The membrane has demonstrated the barrier function of a GTR membrane by thorough separation of the oral epithelial layer from the underlying tissues. In conclusion, we have characterized a biocompatible and bio-resorbable 3D-printed structured gelatin/elastin/sodium hyaluronate membrane with optimal biostability, mechanical strength and surgical handling characteristics in terms of suturability for potential application in GTR procedures.

Keywords: 3D-printing; **Membrane**; Guided Tissue Regeneration (GTR); Soft Tissue Scaffolds; Resorbable Membrane

## 1. Introduction:

Barrier biomaterials have been developed over the past decades for guided tissue regeneration (GTR) which have a wide range of applications in medicine and dentistry.

GTR is a surgical procedure that uses barrier membranes to direct the growth of new tissues at sites with insufficient volumes or dimensions of tissue for proper function, aesthetics or prosthetic restoration [1-3]. While GTR mostly deals with soft tissue, guided bone regeneration (GBR) focuses on separation of bone from the connective tissue [4, 5].

Intraoral applications include regeneration of periodontal bone defects, ridge augmentation prior to dental implant placement in atrophic bone and management of bone defects following trauma, surgical resection of cancer, and repair of cleft palate [2, 6]. Extra-oral applications include orbital floor reconstruction following traumatic fracture of the orbital floor, spinal fusion surgery, orthopedic applications for repair and regeneration of radial bone, rib and femoral bone defects, and neurosurgical applications such as prevention of cerebrospinal fluid leakage from dura mater sites [7].

In addition to favorable biocompatibility and biodegradability, a GTR membrane should have suitable pore size to prevent excessive penetration of oral keratinocytes into the bone defect from one side but allow neovascularization and bone formation from the connective tissue side of the membrane. The three-dimensional topography of the membrane with interconnecting pores and channels is also important to achieve its intended function. Furthermore, the membrane should have good mechanical and handling properties and sufficient tear strength to be able to be sutured and stabilized in place to allow the infiltrated bone cells to differentiate into bone without being disturbed during normal oral function [8]. Mechanical stability facilitates the attachment since it allows additional fixation to be applied to the flexible membranes [9], thereby inhibiting the development of fibrous tissue between the bone and the membrane [10, 11]. It has been observed that bone formation is significantly enhanced when the resorbable membrane is tightly attached and immobilized to the bone surface [12]. Other characteristics of the membrane such as architecture, pore size and permeability can also affect its efficiency. Pore size of a construct has been reported to influence cell adhesion [13, 14] which in turn facilitates coronal migration of the progenitor cells from periodontium in case of barrier membranes since anchorage dependent cells need to adhere to a substrate prior to begin proliferation, migration, differentiation, and maturation [15]. For example, the presence of connective tissue cells on the inner surface of the retrieved membrane has been reported to be predictive of enhanced periodontal tissue regeneration [16]. Cell attachment to the barrier may not only help clot formation and wound stabilization [17], but also stabilize the barrier to diminish membrane micromovement and prevent the disruption of newly formed attachments [18]. Besides, it has been shown that the use of semi-permeable membranes (made of ePTFE) results in a relatively greater speed and quantity of osseous replacement compared to the high-density non-permeable ones. Such a difference has been attributed to the capability of the membranes to exclude cells lacking osteogenic potential and to allow free diffusion of nutrients and growth factors [19].

Non-resorbable membranes initially developed for GTR included expanded polytetrafluoroethylene (e-PTFE) (Gore-Tex® Periodontal Material), titanium reinforced ePTFE (Cytoplast™), high-density-PTFE (TefGen-FD®), or titanium mesh. The main disadvantage of these non-resorbable membranes was the need for a second surgery to remove the membrane. Bio-resorbable membranes were then developed to obviate the need for the second surgery. In addition, such membranes also allow imaging because of their radiolucency as well as reduce stress shielding of the newly formed bone [20]. The most commonly used GTR membranes are made of natural materials such as porcine-derived collagen

membrane (Biogide™, Wolhusen Switzerland). However, there are several limitations associated with the use of collagen-based membranes. These include fast resorption rate and premature loss of material, poor handling characteristics and mechanical strength and risk of disease transmission from animal products and autoimmunization. Synthetic membranes made of various polymers such as poly glycolic acid (PGA), poly lactic acid (PLA), and polycaprolactone (PCL), have been developed to address these issues. However, synthetic bio-resorbable membranes also suffer from lack of control over the resorption rate dictated by factors like local pH and lack of inertness because of unfavorable reactions during degradation [21]. Gelatin-based membranes could be considered as an alternative to collagen ones as gelatin reduces the concerns of immunogenicity and pathogen transmission associated with collagen while provides integrin binding sites for cell adhesion [22]. Other biopolymers and proteins could be added to improve the properties of the membrane. For example, addition of elastin, an extracellular matrix protein, improves elasticity, self-assembly, long-term stability, and biological activity of biomaterials [23] while addition of hyaluronic acid, an essential component of the ECM, may facilitate cellular signaling, wound repair, morphogenesis, and matrix organization [24].

Various techniques are being used for making 3D constructs for specific applications [25-27]. Amongst all of the additive manufacturing methods such as stereolithography (SLA), fused deposition modeling (FDM), and selective laser sintering (SLS) are the most advanced ones, however, the pressure-assisted FDM process is one of the most popular for tissue engineering and bioprinting applications [28-31]. Advances in 3D printing technology have permitted optimization of multiple characteristics of biomaterials for their intended clinical application. Biomaterials, including (i) polymers and ceramics, (ii) natural and synthetic bioplastics, (iii) hydrogels in combination with living cells and/or growth factors, and (iv) proteins and biomolecules, as well as their hybrid structures, can all be printed using these processes [32-35].

For printing biomaterials using pressure-assisted FDM process, the bioink is essentially a material/composite of the appropriate viscosity that is capable of being extruded under pressure through a micro-scale nozzle orifice or a micro-needle [36]. The mechanical integrity of the extruded structures can be controlled through thermal or chemical crosslinking, or multi-material channel approaches post-deposition [37-39]. During the process, the biomaterial is contained in a temperature-controlled cartridge inside a three axis robotic print head with a nozzle or micro-needle. Deposition takes place by pneumatic pressure, plunger or screw-based extrusion of the material as a continuous filament through the nozzle or micro-needle orifice onto a substrate. The substrate can be a solid (e.g., a culture dish), a liquid (e.g., growth media), or a gel-based substrate material. The substrate, as well as the deposition setup, can be contained within a sterile and climate-controlled environment, further enabling the use of temperature sensitive biomaterials. The print head trajectory is guided by layered data obtained from the digital model of the construct to be laid out. The rheological properties of the biomaterial, extrusion temperature, and nozzle type used and the applied pressure are the critical parameters that affect the physical and biological characteristics of the printed construct [38, 40, 41].

Bioinks are an integral part of bioprinting technology [36, 42, 43]. It is not the bioprinting process parameters alone that are important, but also the material-process interactions that govern the viability and success of the resultant constructs. Hence, developing appropriate bioinks and comprehensively characterizing their rheological behavior as well as mechanical, and biological characteristics of the printed construct out of them is critical to the success of bioprinting. It is accepted that this development and characterization will have to be process specific [33, 36].

The aim of this study was to print a structured membrane with optimal physical and biological properties for GTR application. After developing an appropriate bioink, we characterized a biocompatible and bio-resorbable 3D-printed structured gelatin/elastin/sodium hyaluronate membrane. It is known that gelatin is biocompatible, low-cost and cell-attractant, and sodium hyaluronate improves chemical signaling among cells [44-46]. Elastin may also benefit long-term stability, elasticity, and biological activity of the membrane [44]. The optimal biostability, mechanical strength, surgical handling characteristics and in vitro biocompatibility to be used for GTR surgical procedures have been explored in this paper.

## 2. Materials and Methods

### 2.1. Materials

Elastin with molecular weight 60KDa (Elastin-Soluble, No. ES12) was purchased from Elastin Products Company, Inc. (USA). Sodium hyaluronate (Research Grade, 500KDa-749KDa) and gelatin (Type A, from porcine skin, Bioreagent grade) were obtained from Lifecore Biomedical (USA) and Sigma-Aldrich (USA), respectively. 1-Ethyl-3-(3-dimethylaminopropyl) carbodiimide (EDC) and N-Hydroxysuccinimide (NHS) were purchased from Alfa Aesar (USA).

Penicillin, streptomycin, amphotericin B, complete Dulbecco's Modified Eagle Medium (cDMEM), ascorbic acid were purchased from Sigma-Aldrich (UK). Collagenase type I solution was obtained from Gibco (USA) and prestoblue (PB) assay was purchased from Invitrogen (UK).

### 2.2. Optimizing the formulation of the bio-ink and membrane printing

To select the most suitable composition of materials, seventeen different aqueous solutions of gelatin, elastin and sodium hyaluronate were prepared (described in Appendix 1). Each solution was molded into a 24 well plate dish (150  $\mu$ l in each well). After crosslinking with 6 mg/ml EDC and 0.75 mg/ml in 70% ethanol for 0.5-2 hour, molded thin membranes with the approximate thickness of 200  $\mu$ m were obtained and washed with a large amount of deionized (DI) water. Using a surgical suture kit, the ability of the prepared membranes to be sutured was examined. The ones with good results underwent rheology analyses to find the most appropriate bio-ink for the printing. More specifically, three solutions with the compositions described in Table 1 were selected for the rheology analyses.

Table 1: Sample specification for the primary rheometry experiment. The w/v refers to the weight of the materials in DI water.

	Gelatin concentration (w/v)	Elastin concentration (w/v)	Sodium hyaluronate concentration (w/v)
Sample 1	15	-	-
Sample 2	15	2	0.5
Sample 3	8	2	0.5

The gel point of different solutions was measured using a Malvern Kinexus rheometer with disc (D=20 mm) and parallel plate geometry. The distance between the disc and plate was adjusted to be 0.3 mm. Oscillation and viscometry experiments were conducted at different temperature ranging from 20 to 40°C. Oscillatory shear measurements were performed in the linear viscoelastic regime (shear strain 2%) where the storage and loss modulus are independent of the strain amplitude.

Scanning from high temperatures to low temperatures, different frequencies were scanned at each temperature. The sample with the closest gel point to room temperature was selected as the bio-ink to be printed. The rest of the experiment was carried out for the constructs printed using selected bio-ink.

After optimizing the ink composition, EnvisionTEC 3D-Bioplotter® (Manufacturer Series, Germany) was employed for the 3D printing of scaffolds. The camera of the 3D-Bioplotter® was utilized for the imaging of each layer during the process.

The selected solution was printed at material container temperature of 30-32 °C, platform temperature of 11 °C, printing pressure of 0.6-1.2 bar, speed of 20 mm/s using 250 µm-diameter needle. Pre- and post-flow delays were set to zero. Each membrane contained 6 layers with strand angles of 45, 135, 0, 90, 0, 90° for layers 1 to 6, respectively. Distances between strands were set to 0.6 µm for the first 4 layers and 0.9 µm for the last 2 layers. Hardening of the ink happened almost immediately after being dispensed from the needle and touching the platform through the capability of the solution to form a solid gel at lower temperatures. The 3D-printed membranes were cross-linked by soaking them in 6 mg/ml EDC and 0.75mg/ml NHS in 70% ethanol for 0.5-2 h. To remove the residual cross-linker, the membranes were washed carefully through soaking them in a large amount of DI water (500 ml) for 1.5 h. The water was replaced with fresh water every 0.5 h. The prepared membranes were stored in 100% ethanol inside a -20 °C freezer to be used after rehydration when needed.

### **2.3. Morphology, surface roughness and thickness of the membranes**

A Dino-lite digital microscope camera was employed to obtain low magnification photos of the membranes after complete preparation. LEXT OLS4000 3D Laser Measuring Microscopy (Olympus, Japan) was used for imaging of the membranes. Moreover, the surface morphology and roughness was analyzed using the 3D Laser Measuring Microscopy. The thickness of the membranes was measured using a Marathon Electronic Digital Micrometer. The thickness values were confirmed by scanning the edge of the membrane using the 3D Laser Measuring Microscope.

### **2.4. Static and dynamic mechanical properties**

Static tensile properties of the membrane were measured using a universal tester (AGS-X 5kN, Shimadzu). For this purpose, the samples cross-linked for 0.5 h were fixed into screw flat tensile grip and underwent tensile test using a 1 kN load cell and crosshead speed of 1 mm/min. Dynamic mechanical analyser (DMA 8000, Perkin Elmer) was used to measure the dynamic tensile storage modulus of the printed membranes after cross-linking for 0.5 h. The samples were sized into small pieces appropriate for the DMA analysis (approximately 5.0 mm × 5.0 mm). The samples were analyzed in tension mode while soaked in a fluid bath. The frequency sweep from 0.1 to 25 Hz was conducted at a dynamic displacement of 0.05 mm.

### **2.5. Degradation**

The degradation rate of the samples (15 mm × 15 mm) with different cross-linking times (i.e. 0.5, 1.5, 2 h) were measured through immersing the samples in 10 ml Phosphate-buffered saline (PBS) each and storing them in a shaking incubator at 37 °C. First, the initial weights of the samples were recorded. Then, at certain time intervals, samples were taken out and their weights were recorded after excess water was removed. The ratio of the weight of each sample at that time point to the initial weight of the sample was reported against the time of immersion (weight loss). The measurements were performed until complete collapse of the samples.

## **2.6. Tissue collection**

Keratinized gingival biopsies (5×5 mm) were obtained from patients undergoing oral surgery with their informed written consent at the Charles Clifford Dental Hospital, Sheffield under ethical approval granted by the Sheffield Research Ethics Committee (15/LO/0116, STH Research Department: STH18551). The specimens were collected in sterile PBS and transported on the same day to the laboratory for processing.

## **2.7. Cell isolation and culture**

Tissues were rinsed and disinfected three times with PBS supplemented with 50 U.ml<sup>-1</sup> penicillin, 50 U.ml<sup>-1</sup> streptomycin and 625 ng.ml<sup>-1</sup> amphotericin B. Normal oral fibroblasts (NOF) and normal oral keratinocytes (NOK) were enzymatically isolated from oral biopsies as previously described [47]. Briefly, NOK were isolated by incubating the tissues in trypsin in PBS (1:250) for 1 hour at 4°C and then 2 hours at 37°C. The epithelial layer was scraped and the tiny pieces were plated in a T-25 tissue culture flask, allowed to adhere for 15 minutes, and then cultured in Green's medium [48] at 37°C in a humidified and 5% CO<sub>2</sub>/95% air atmosphere. The medium was changed every two days until the cells were 90% confluent. The cells were then sub-cultured as mentioned above and used after the first passage.

NOF were isolated from the connective tissue layer of the remaining oral mucosa biopsy by incubation in 0.05% (w/v) collagenase type I solution in cDMEM at 37 °C overnight. Digested tissue was centrifuged at 200 rpm for 5 minutes and the pellet was re-suspended in cDMEM and cultured in a T-75 cell culture flask. The medium was changed 2-3 times a week until the cells were 90% confluent when they were sub-cultured and used following the second passage.

## **2.8. Membrane cell seeding**

Membranes sized 15mm × 15mm (N=6) were washed 3 times with PBS prior to the experiment and each scaffold was placed in 3 cm diameter hanged cell culture inserts. Then, NOF 0.5×10<sup>6</sup> cells/scaffold were seeded onto the large pore-size side and after 4 hours NOK 10<sup>6</sup> cells/scaffold were seeded onto the small-pore size surface. The culture media used was cDMEM supplemented with 50 µg/ml ascorbic acid in the outside of the insert (2 ml) and Green's M inside the insert (2 ml). The medium was changed every other day. After 4 days, the constructs were lifted to the air liquid interface (ALI) and following 12 days at ALI, two of the constructs were fixed in 10 % formalin and paraffin embedded sections were prepared for histological examination. The remaining constructs were further cultured for another 4 days for tissue viability assay as described below.

## **2.9. Cell Vitality**

Cell vitality was assessed after 2, 10, and 20 days of culture (after initial cell seeding) using PB assay. At each time point, the constructs were washed 3 times with PBS before 900 µl of serum free medium with 100 µl of PB reagent added to each insert. After 3 hours of incubation, 200 µl in triplicate were aspirated from each model for fluorescent reading using a spectrophotometric plate reader (Infinite® M200,TECAN, USA) at 560 nm excitation and 590 nm emission. The statistic was performed using GraphPad Prism 7. The difference was considered significant at P-value< 0.05 using the one-way ANOVA test.

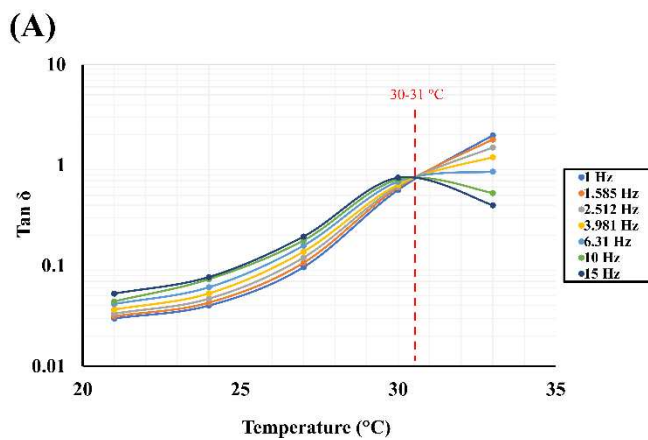
## **2.10. DAPI nuclei staining**

Frozen sections (8  $\mu\text{m}$ ) of the membranes with cells were prepared and the slides were washed with PBS 3 times and mounted using mounting medium containing 4,6-diamidino-2-phenylindole (DAPI) stain (Sigma Chemical Co.) and assessed under a fluorescence microscope (BX51, Olympus, Tokyo, Japan).

### 3. Results and Discussion:

#### 3.1. Ink optimization

For thermoreversible gels, the gel point can be defined as the temperature at which the loss tangent (dissipation factor,  $\text{Tan } \delta$ ) is independent of frequency [49]. Therefore, the gelation temperature of a solution can be acquired through a multi-frequency plot for a temperature sweep measurement. Loss tangent ( $\text{Tan } \delta$ ) of gels of different compositions against temperature has been plotted at different frequencies in Figure 1.



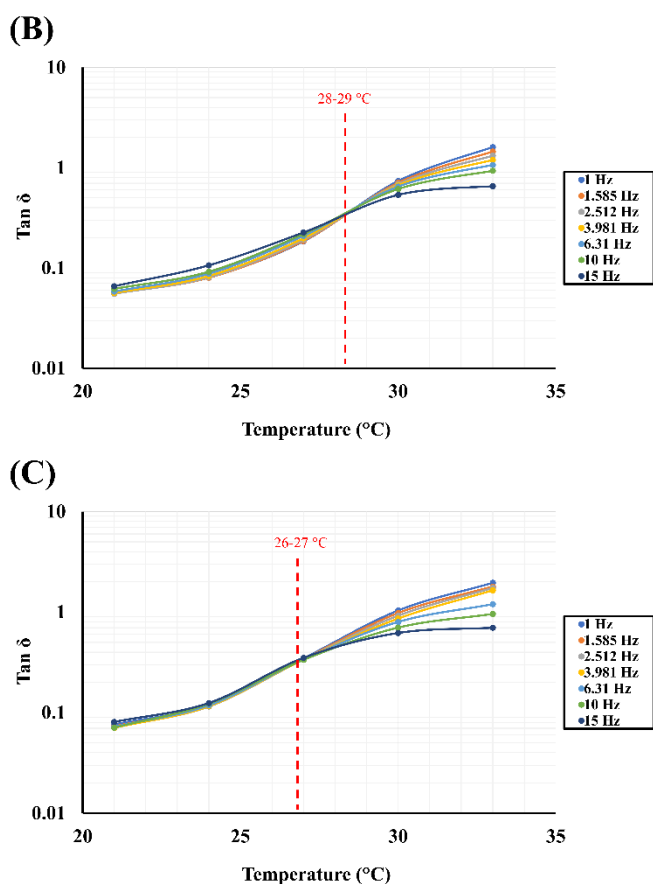


Figure 1: Loss tangent vs. temperature plotted in different frequencies for (A) gelatin 15%, (B) gelatin 15% elastin 2% sodium hyaluronate 0.5%, and (C) gelatin 8% elastin 2% sodium hyaluronate 0.5%

The gel point of the gelatin-containing solutions is important in the printing process. For fused deposition modeling of such solutions, it is necessary to have them in sol (liquid) state in the cartridge and needle while a sol-gel transition is required to maintain the shape on the platform after printing. The transition should be fast enough to prevent any flow after the material is printed on the platform. To do this, the cartridge containing the ink could be heated above the gel point while the platform temperature is kept below the gel point. In this case, the closer the cartridge temperature to the gel point and the further the platform temperature is away from the gel point, the faster the gelation process will be. However, there are some key issues in practice that need to be addressed for successful printing:

- The needle is in contact with room temperature when the printer is in stand-by mode. Therefore, there is always a temperature gradient between the cartridge and the needle. In this case, if the needle temperature falls below the gel point, the needle will be clogged through gelation and the material can't be printed.
- If the cartridge temperature is increased far above the gel point in order to manage the temperature gradient mentioned earlier, two possible problems may occur; firstly, the high temperature of the sol postpones the gelation on the platform; secondly, the pressure that should be used to initiate the ink flow is too high for printing because of the difference between the needle and cartridge temperatures. At the beginning, the pressure should be high enough to overcome the needle-contained ink resistance to flow but once the flow is achieved, such pressure is too high to be used for printing the strands. This happens because the viscosity of the solution highly depends on the

temperature as shown in Figure 2. Lower temperature of the needle results in higher viscosity and the need to use higher pressure to start. However, as the needle content is completely printed, such high pressure is no longer required and it may cause overflow onto the platform.

- As the printing is in progress, the needle is in contact with the material printed on the platform in previous cycles. In this case, the needle temperature may drop below the gel point which causes the needle to be clogged in the middle of the printing process.

Minimizing the temperature gradient between the material in the cartridge and the needle was found to be an effective strategy to eliminate such problems. It can be performed by adjusting the gel point to be close to room temperature to prevent gelation in the needle. Changing the concentration of gelatin as the main component of the formulation and addition of elastin and sodium hyaluronate was found to be effective for adjusting the gel point.

As can be seen in Figure 1, the gel point of 15% gelatin solution was found to be between 30-31 °C. Addition of elastin and sodium hyaluronate to 15% gelatin solution resulted in a decrease of the gel point to 28-29 °C. The gel point was further decreased by reducing the concentration of gelatin to 8% while keeping the concentration of elastin and sodium hyaluronate constant. It was decreased to 26-27 °C (Figure 1) which is close enough to room temperature for printing. This gave us a good reason for choosing 8% gelatin/ 2% elastin/ 0.5% sodium hyaluronate as the ink for the 3D printing.

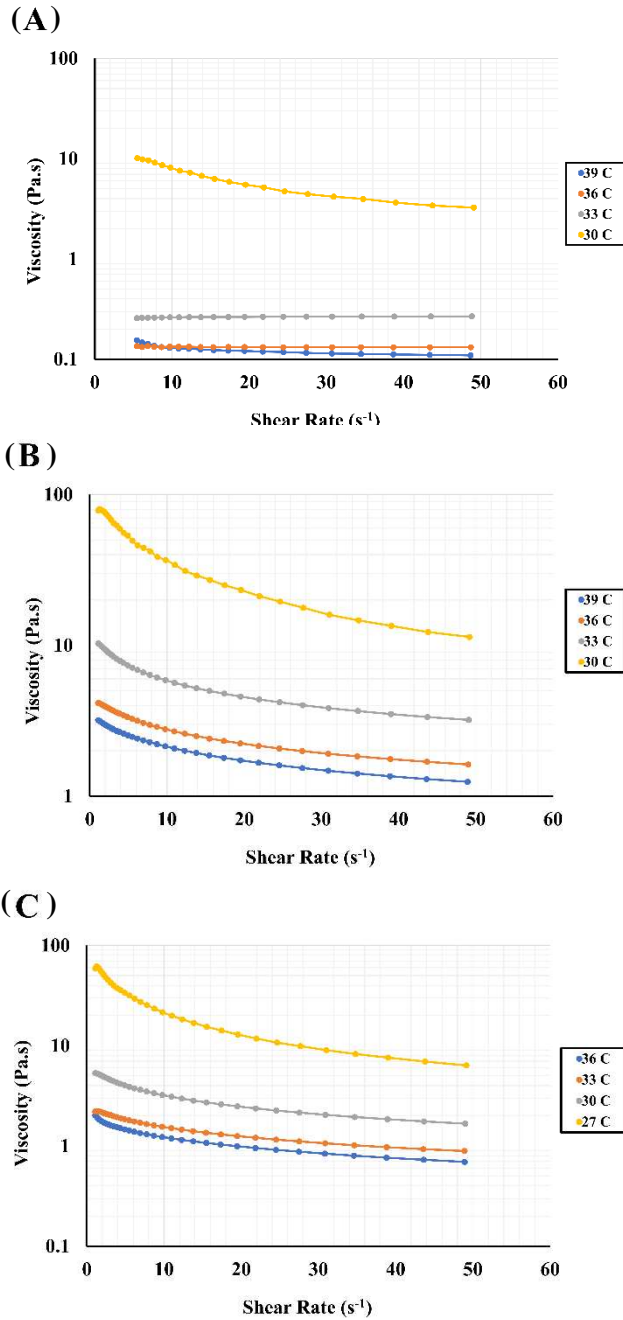


Figure 2: Viscosity vs. shear rate plotted in different temperatures for (A) gelatin 15%, (B) gelatin 15% elastin 2% sodium hyaluronate 0.5%, and (C) gelatin 8% elastin 2% sodium hyaluronate 0.5%

Viscosity of the ink is an important parameter for reproducing the printing process and determining the printing variables such as pressure and speed. Very low or high viscosity makes the solution unprintable. Figure 2 presents the values of viscosity for our solutions. As can be seen in the figure, gelatin-based solutions represent a shear-thinning behavior in sol state. The viscosity highly depends

on the temperature especially in temperatures closer to the gel point which shows the importance of the temperature of the cartridge in the printing process.

At a specific temperature, addition of 2% elastin and 0.5% sodium hyaluronate to 15% gelatin solution results in a significant increase in viscosity. On the other hand, decreasing the gelatin concentration from 15% to 8% causes a decrease in viscosity. In the printing procedure, the cartridge temperature was set to 30-32 °C that corresponded to viscosity values between 1-10 Pa.s. A solution with such viscosity can be printed using the applied pressure, speed and platform temperature to yield a reproducible well-ordered membrane.

### **3.2. Morphology, surface roughness and thickness of the membranes**

Sample preparation is the main difference between using the 3D Laser Measuring Microscopy and SEM. No sample preparation is needed for the 3D Laser Measuring Microscopy and the imaging can be performed under room conditions while the membranes are in their original shape. Since the SEM has to be conducted under vacuum conditions and the samples have to be coated with a conductive material, the samples are slightly deformed and the images do not represent the exact shape of the construct. Although, the resolution of the SEM is better than the 3D Laser Measuring Microscope, the latter was good enough for our purpose.

Figure 3 A-C schematically represents the architecture of the printed membranes. The membrane was printed with gradient structure; i.e. one side had small pores to prevent connective tissue invasion and the other side had larger pores to allow potential epithelial cell/bone growth. Crosslinking helped to keep the structural integrity of the 3D-printed membrane. Based on our visual observations, the handling of non-crosslinked membranes was difficult and they collapsed easily. The degradation resistance of the hydrogels could be improved significantly by crosslinking.

Regarding the design of the membrane, in a novel configuration, to be able to effectively grow one type of tissue (e.g. epithelial tissue) on one side of the membrane and another type of tissue (e.g. connective tissue/bone) on the other side, we made a gradient membrane with different structures on each side. This model could mimic a real tissue interface which has dissimilar tissues on each side. One side of the membrane had very large pores (400-500 µm) so we could seed cells that could easily grow on the membrane. On the other side, the pore size was smaller (50-150 µm). Our experiments showed that this pore size made a barrier thin layer that prevented keratinocytes from dropping into the other side, which is a necessary feature for the membrane to facilitate guided tissue regeneration (GTR). It is important to note that maintaining the permeability of the membrane is essential since it allows nutrient diffusion and healthy cell growth and differentiation.

Figure 3 D-E shows the macroscopic images of the prepared 3D-printed membranes. As can be seen in this figure, the membranes were flexible. We also found that they offer easy surgical handling [50]. The thickness of the membrane, based on the measurement with the Electronic Digital Micrometer was approximately 100-200 µm. Note that if the crosslinking was done immediately after the 3D printing, the thickness was larger (toward 200 µm). Prolonged waiting time after 3D printing and before crosslinking yielded thinner membranes (toward 100 µm).

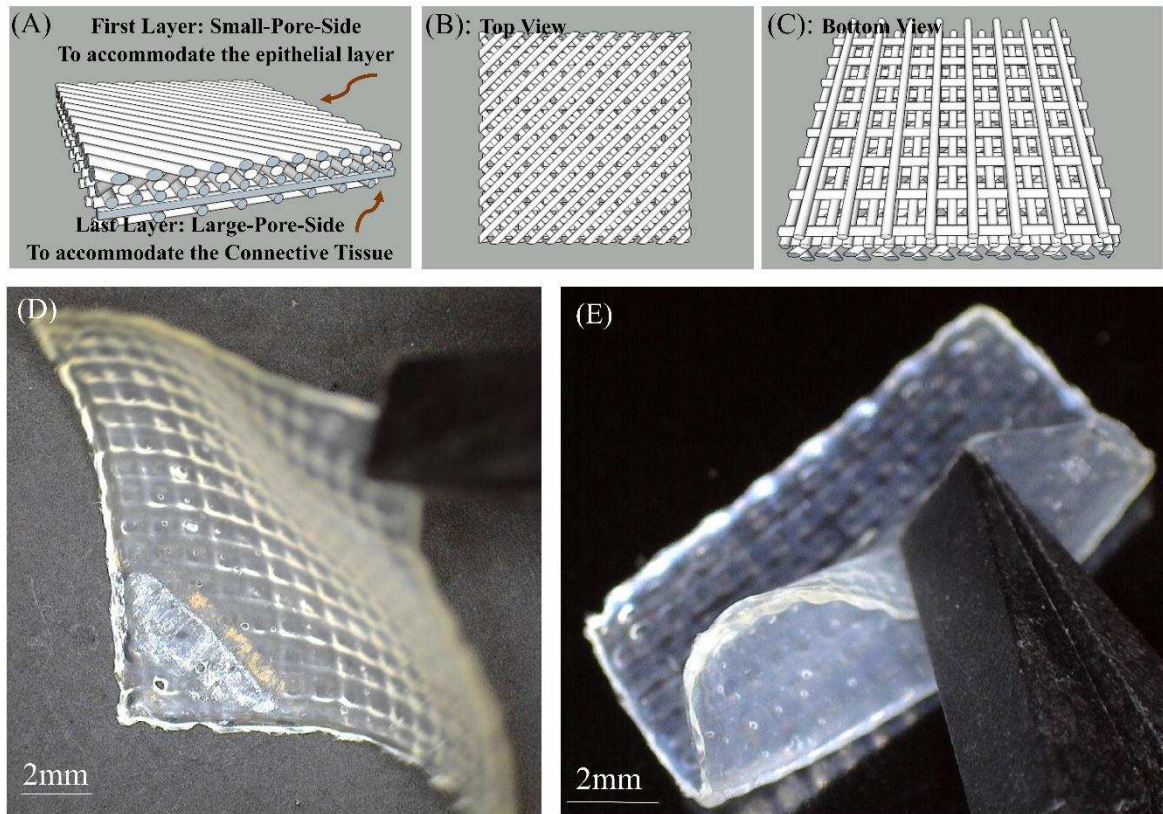


Figure 3: (A-C): Schematic of our design. Each membrane is composed of 6 layers. The strand angles from the first layer to the last layer are: 45, 135, 0, 90, 0, 90°. Distances between strands (from the middle of one strand to the middle of the adjacent one) are set to 0.6  $\mu\text{m}$  for the layers 1-4 and 0.9  $\mu\text{m}$  for layers 5-6. (D-E): The macroscopic view of the 3D-printed gradient membranes of gelatin/elastin/sodium hyaluronate. The membranes are completely flexible and bendable. The surgical handling of the membrane is easy. The thickness is approximately 150  $\mu\text{m}$ .

To store the membrane, having it in 100% ethanol inside a freezer was very effective and it seems the membrane can keep its functionality forever if it is stored this way (we have tried it for several months without seeing any change in the quality of the membrane). In contrast, the membranes were completely hard, fragile and not flexible when kept in ethanol due to the dehydration. Because of the thin structure, by soaking the dehydrated membranes in water, they became flexible in 30 seconds and were the same as the original in terms of shape and quality. We have not seen any visual change in the membranes by soaking them in water for a longer time and it seems that they can be fully swelled in a very short time.

Figure 4 presents high magnification images of the two sides of the membrane taken by the 3D Laser Measuring Microscope. The first layer had small pores and the last layer was designed to contain large pores. The roughness of the two sides were different. The value of the roughness was not fixed in different membranes but the small-pore-side was always significantly smoother than the large-pore-side. The average values of the roughness ( $R_a$ : Arithmetical mean deviation of the roughness profile) of the small-pore-side and large-pore-side were measured at around 0.30 and 1.19  $\mu\text{m}$ , respectively.

The images in Figure 4(A, B) were taken when the membrane was in the fully swelled state (i.e. just taken out from the water). After about half an hour keeping the membrane under the microscope,

the membrane became slightly dry and the pores of both sides can be seen from the top view (from the small-pore-side) under the microscope, as shown in Figure 4(C). As displayed in this figure, the small pores were around 140  $\mu\text{m}$  in this membrane and the large pores were around 440  $\mu\text{m}$ . In different membranes, the sizes of small pores were measured to be between 50-150  $\mu\text{m}$  and the size of the large pores was usually very close to 450  $\mu\text{m}$ .

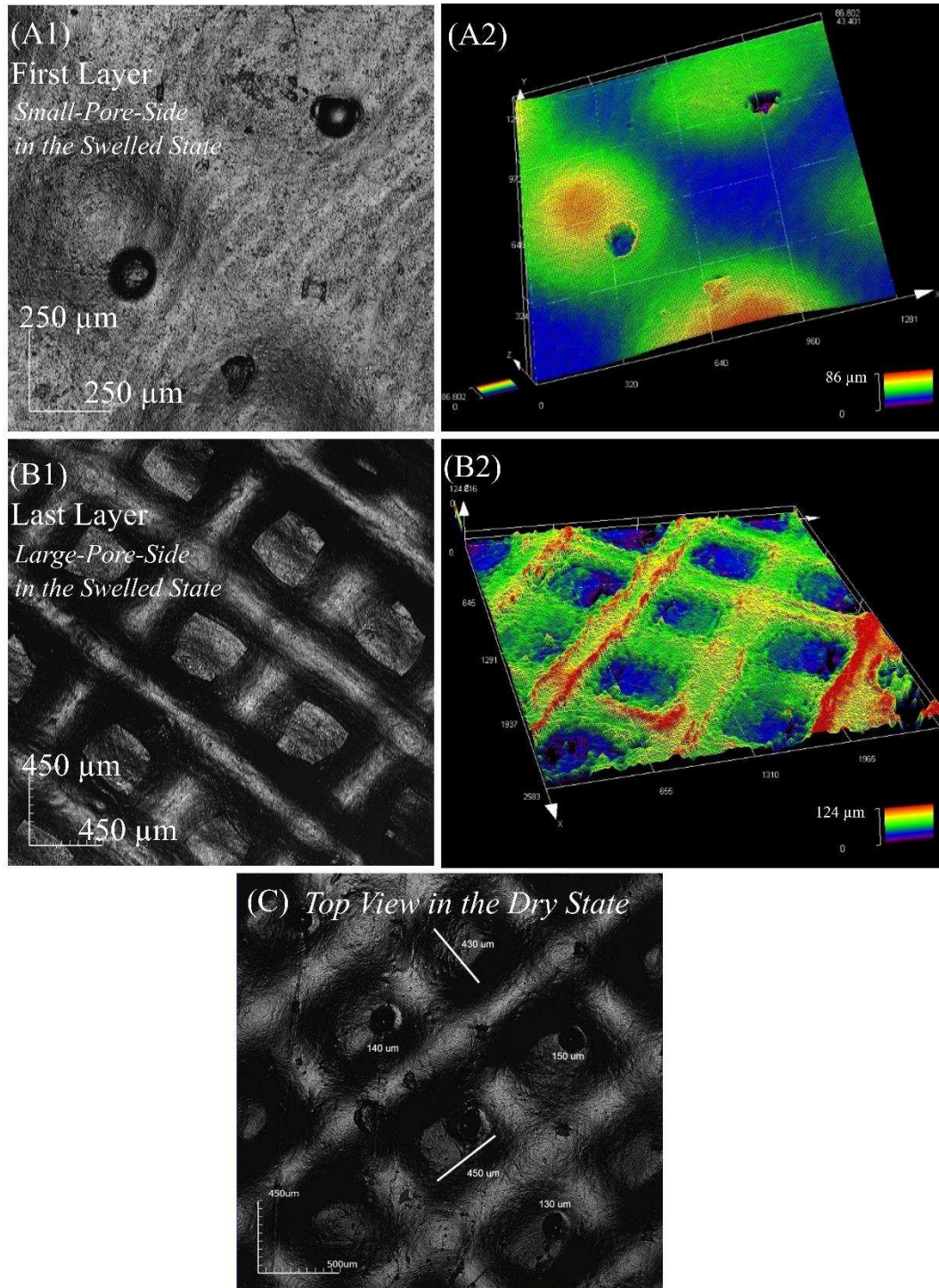


Figure 4: 3D Laser Measuring imaging of the scaffolds from both sides of the sample composing of gelatin 8%, elastin 2% and sodium hyaluronate 0.5%. (A1, B1): imaging of the small-pore-side and large-pore-side in a completely swelled state. (A2, B2) the height profile and surface morphology of

the images in panel A1 and B1. The Red area. Small-pore-side has smoother surface than the large-pore-side. The color coding indicates the height in  $\mu\text{m}$ . (C). Both sides of the membrane can be visualized under the 3D Laser Measuring Microscope after drying the sample by 30 minutes keeping a fully swelled membrane under room conditions (C).

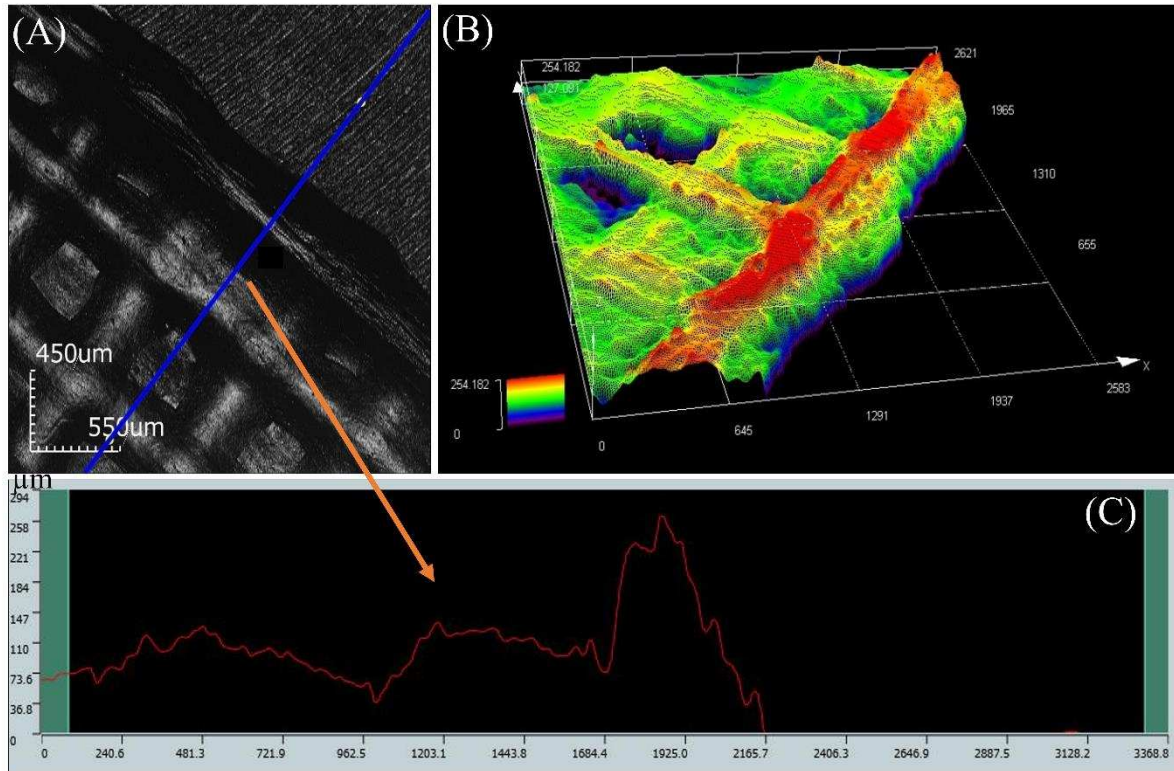


Figure 5: A) The 3D laser imaging of the membranes to confirm the thickness of the membranes measured by the Electronic Digital Micrometer. B) The height profile of the edge of the membrane. C) The line height scan of the blue line in panel A. The edge of the membrane is a bit higher than the actual surface as the printer was set to do the contouring after each layer of printing.

Figure 5 shows the laser scanning of the edge of the membrane to have more detailed information about the thickness of the membrane. As seen in this figure, although right at the edge, the membrane was thicker; the overall thickness of the membrane was approximately  $150 \mu\text{m}$ , which confirmed the Electronic Digital Micrometer measurement. Having thicker edge is a result of printing a contour for each layer in every printing cycle by the 3D-printer. The contour is a solid printed line that verifies the margins of the printed object in each layer. Printing a contour supports the integrity of the membrane while making the edge thicker as the strands are stacked on top of each other in this region.

### 3.3. Static and dynamic mechanical properties

The tensile static mechanical testing of the membranes ( $15 \text{ mm} \times 15 \text{ mm}$ ) cross-linked for 0.5 h revealed a tensile modulus of  $1.95 \pm 0.55 \text{ MPa}$  (Figure 6). Maximum stress of  $1.15 \pm 0.33 \text{ MPa}$  could be applied to them, where the maximum elongation at breaking point was  $60 \pm 7\%$  of the initial length. Figure 6 shows a sample force-displacement graph of the membrane. As can be seen, the membrane exhibited elastic (linear) behavior until it was ripped.

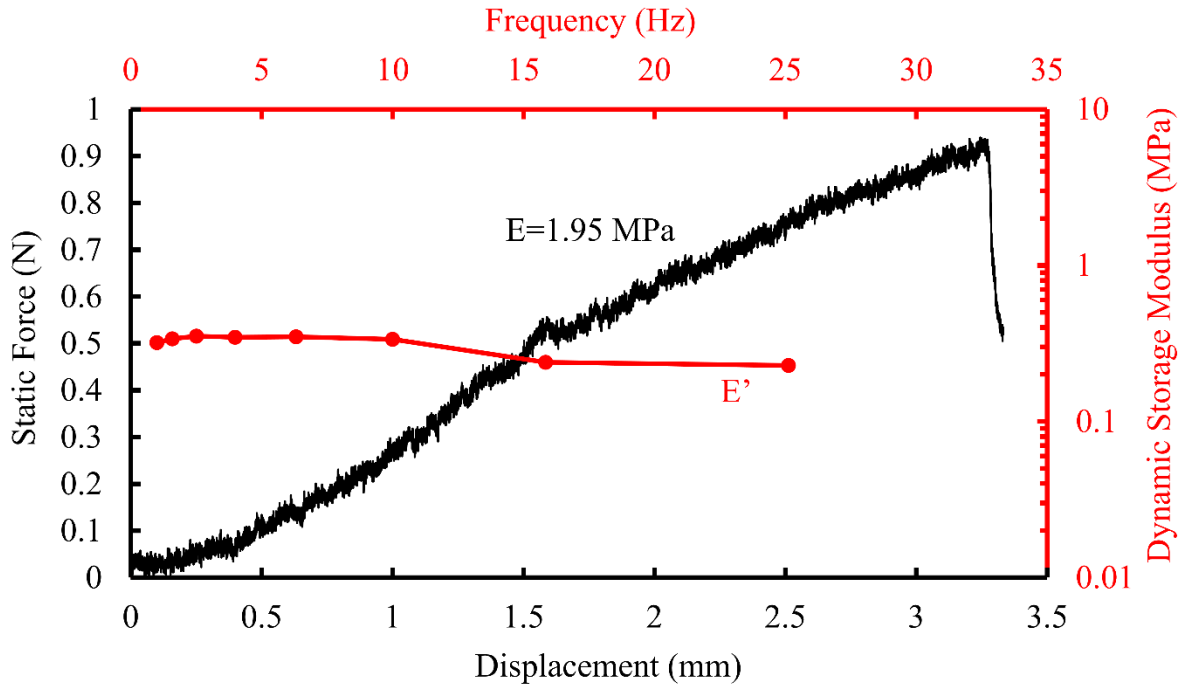


Figure 6: Static mechanical testing revealed elastic modulus of  $1.95 \pm 0.55$  MPa (black); dynamic storage modulus vs. frequency for printed membranes (red). The measured dynamic storage modulus was  $314 \pm 50$  kPa and had not been significantly altered by increasing the frequency.

DMA was used to measure the dynamic storage modulus of the printed membrane after crosslinking for 0.5 h. The frequencies in the range of 0-25 Hz were swept at room temperature. The results are shown in Figure 6. As can be seen, the storage modulus does not change significantly with frequency change in the scanned range. Note that increasing the temperature to 37 °C did not have a significant impact on the storage modulus. The tensile storage modulus was found to be  $314 \pm 50$  kPa.

### 3.4. Degradation

Figure 7 shows the degradation profile of the samples in PBS at 37 °C. The effect of cross-linking time can be vividly observed in this figure. Increasing the cross-linking time from 0.5 h to 1.5 h, prolonged the degradation resistance for more than 10 days. Longer cross-linking times up to 2 h further increased the degradation time of the samples to more than a month. The membranes kept their integrity and whole weight for a certain period and collapsed suddenly at the next time points. As can be seen, membranes cross-linked for 0.5 h swelled through being immersed in PBS and maintained a portion of their water content up to the end point of the experiment (weight/initial weight > 1). However, increasing the cross-linking time resulted in decreased swelling that was a result of augmentation of cross-linking density. It is worth mentioning that the longer the cross-linking time was, the less flexible the membrane became. The resorption rate of the membrane is important since it affects the success of regeneration. For example, the membrane should function 4-6 weeks before resorption to allow successful regeneration of the periodontal systems [4]. Monitoring changes in pH of the PBS or the weight of the sample over time is commonly used to track the degradation of biodegradable materials such as PLGA [51], collagen, gelatin and elastin [52] which provide the information about the kinetics of hydrolytic degradation.

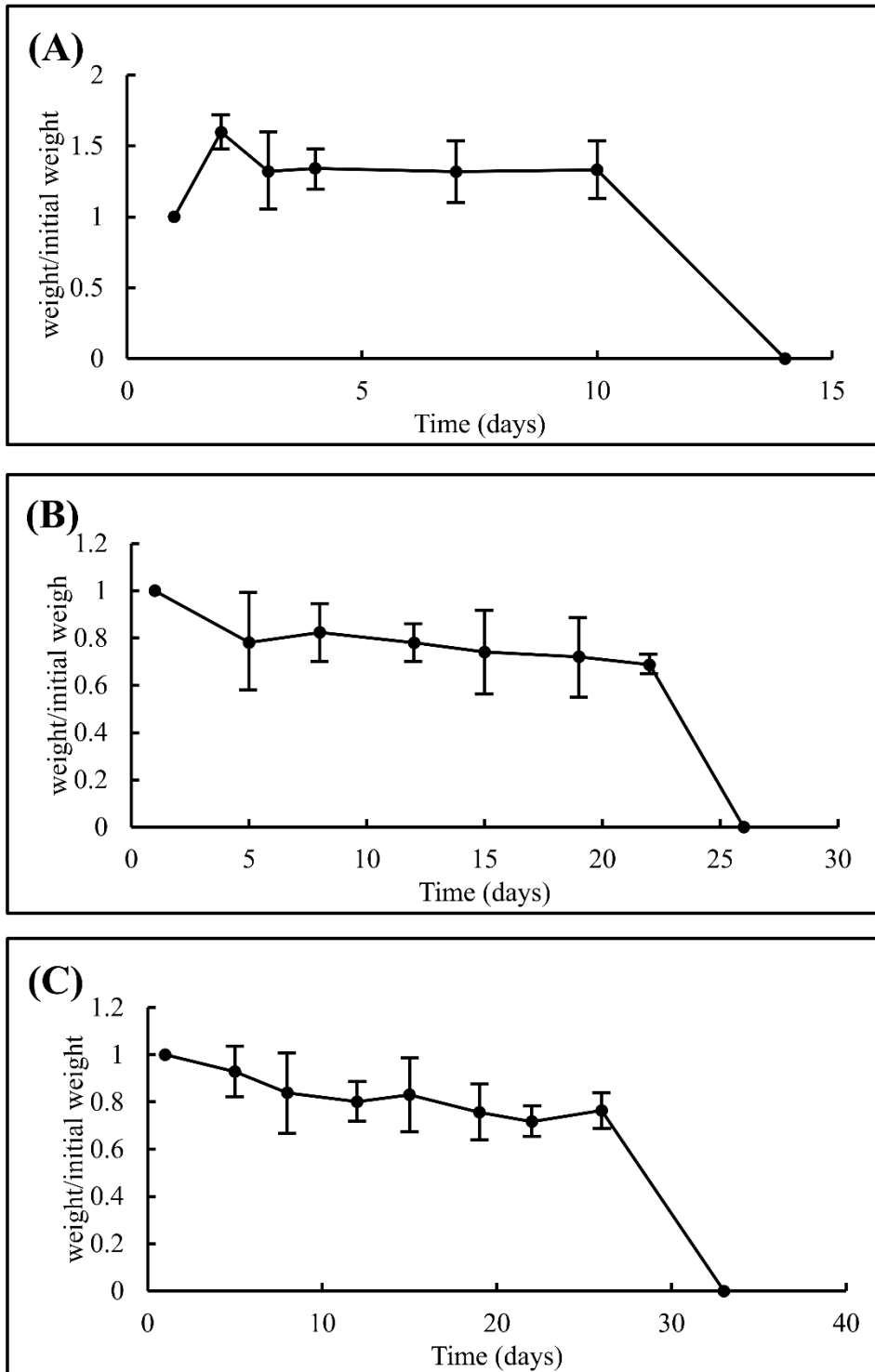


Figure 7: **Degradation** rate of the membranes crosslinked using EDC/NHS for 0.5 h (A), 1.5 h (B) and 2 h (C). The membranes were soaked in PBS at 37 °C for this experiment.

### 3.5. Biological evaluation in vitro

Histology allows us to visualize and directly assess any potential toxicity and cell damage on the epithelial cells caused by the materials in the membrane. This can be quantified by using a cell viability assay which has been employed in this study. The ability of the GTR membrane to separate

different cells grown on different sides of the membrane can also be assessed using histological evaluation of the constructs.

Figure 8 demonstrates the histological sections of the 3D-printed membrane before and after cell seeding and culture. Oral keratinocytes proliferated and formed an epithelial layer on the surface of the 3D-printed membrane with no sign of invasion into the deeper layers of the membrane showing the optimal barrier function of the membrane. Oral fibroblasts also proliferated on the other side of the membrane and formed multilayers of cells separated from the epithelial layer by the membrane.

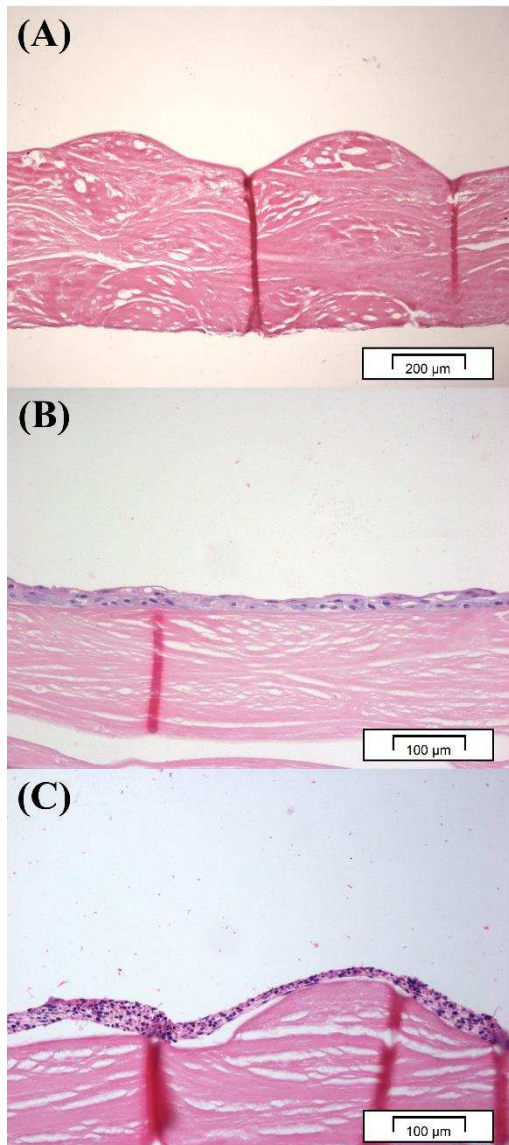


Figure 8: Histological sections of paraffin wax-embedded constructs cultured at submerged condition for 4 days followed by air-liquid interface culture for 12 days. (A) acellular 3D-printed membrane; (B) the epithelial side of the 3D-printed scaffold with cultured NOK forming multilayers at the surface of the membrane without invading deeper into the membrane and (C) the connective tissue side of the scaffold with cultured NOF showing abundance of fibroblast cells nicely separated from the epithelial layer by the GTR membrane. Hematoxylin and Eosin staining, original magnification  $\times 100$ . Vertical lines are due to folding of the sections.

The prestoblu (PB) assay incorporates a fluorometric/colorimetric growth indicator based on detection of metabolic activity. The system incorporates an oxidation–reduction indicator that both fluoresces and changes color in response to chemical reduction of growth medium resulting from cell growth. PB has two advantages: first, its change in color can be detected both spectrophotometrically and fluorometrically, which gives greater sensitivity of detection; second, since it is not toxic to the cells, it is possible to assess cell viability on more than one occasion. The results of the PB tissue viability assay at days 2, 10 and 20 following seeding of the membranes are demonstrated in Figure 9. The cells maintained their vitality throughout the culture period on the 3D-printed membrane. It appears that after day 10 the proliferation rate had reached a plateau which is expected for oral epithelial cells as they start to differentiate at the air-liquid interface culture.

Although cellular vitality persisted in vitro for 3 weeks, our quantitative investigations revealed a small decrease in cellularity after 10 days which may indicate reduction in cell proliferation. This may be attributed to the limitations of the static culture condition used in this study as the dominant nutrient exchange within the construct remains by diffusion. Furthermore, mucosal cells have a high proliferation rate and nutritional demands which can result in early deprivation from nutrients and cell death which was noticed in this study towards the end of the culture period.

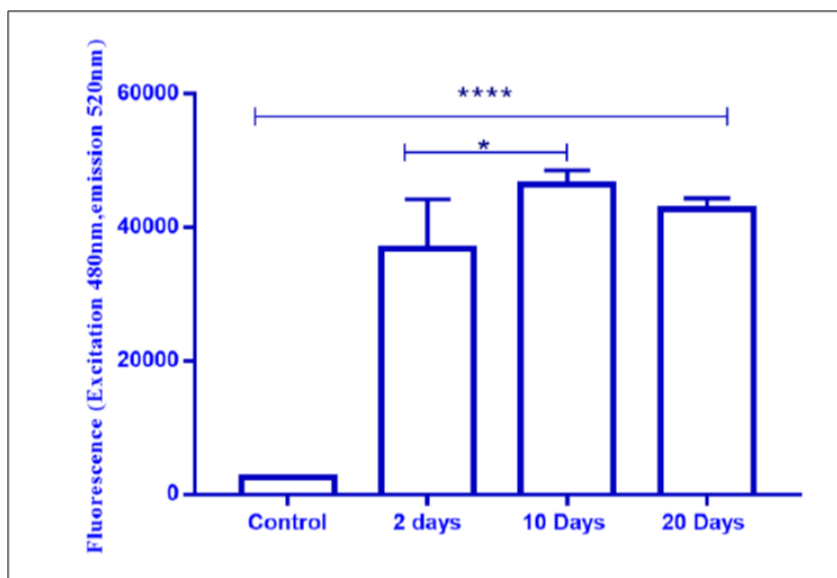


Figure 9: Viability of the membranes seeded with oral fibroblasts and keratinocytes at different culture intervals as assessed by the prestoblu PB assay (assay has been performed after seeding of both cell types i.e. 2 days, 10 days and 20 days)

DAPI is a fluorescent stain that binds strongly to A-T rich regions in DNA and is used extensively in fluorescence microscopy to visualize the cell nuclei. DAPI staining was used in this study to identify any invasion and penetration of the oral keratinocytes into the GTR membrane.

Figure 10 demonstrates DAPI stained cell nuclei on the surface of the 3D-printed membrane. The shiny cell nuclei were only visible on the surface of the membrane and were not detected within the membrane showing an ideal barrier function of the GTR membrane tested in this study.

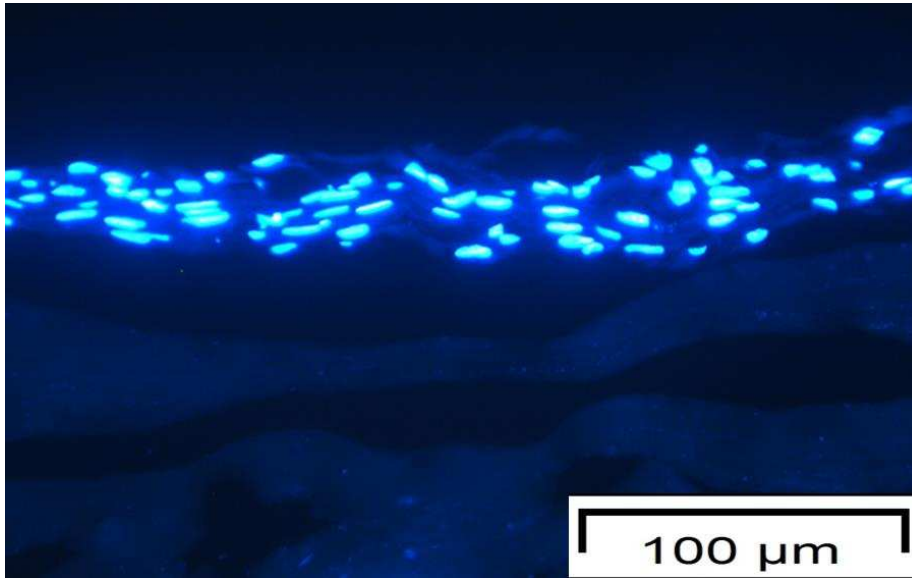


Figure 10: DAPI-stained image of the frozen sectioned construct cultured at submerged condition for 4 days followed by air-liquid interface culture for an additional 12 days showing the nuclei of the cells cultured on the 3D-printed membrane forming multilayers at the surface and absence of any cell nuclei within the membrane confirming its desirable barrier function.

The results of the *in vitro* tests in this study indicated that the 3D-printed membrane had good biocompatibility as assessed by histology and tissue viability assays. Both human oral fibroblasts and keratinocytes were compatible with the membrane and proliferated and attached to the material. The epithelial cells formed a continuous epithelium on the surface of the membrane with no signs of epithelial invasion into the deeper layers of the biomaterial as confirmed by DAPI staining. This suggested that the 3D-printed membrane was able to achieve the desired barrier function of a GTR membrane *in vitro* by complete separation of the oral epithelial layer from the underlying tissues allowing growth and proliferation of the other cell types under the connective tissue layer. These findings have not previously been reported and this is the first study indicating the suitability of a 3D-printed hybrid scaffold for potential application in guided tissue regeneration. Further *in vivo* studies are underway to assess the *in vivo* biocompatibility and biodegradability of the hybrid material and to optimize the surgical technique for the use of this 3D-printed GTR membrane for different oral soft and hard tissue augmentation procedures.

#### 4. Conclusion:

Engaging a 3D-printing method, we manufactured a novel structured soft membrane for GTR application made of gelatin, elastin and sodium hyaluronate. The rationale behind focusing on these three components to make the **membrane** was the fact that gelatin can act as a fibroblast-attractant, elastin has long-term stability, elasticity and biological activity, and sodium hyaluronate facilitates

chemical signaling among cells. After performing the rheology analyses on several different compositions of these three components, we selected a specific composition of 8% w/v gelatin, 2% w/v elastin and 0.5% w/v sodium hyaluronate as the most suitable and printable bioink which resulted in a membrane with appropriate mechanical property. The printed membrane was composed of 6 layers with gradient structure. This design allowed us to have two different sides with large and small pores ideal for different types of cells. 3D Laser Measuring was a useful technique employed for imaging of the membrane to confirm the structures and pores on different sides.

The optimized membrane had the desirable thickness (150  $\mu\text{m}$ ), static tensile modulus ( $1.95 \pm 0.55$  MPa) and dynamic tensile storage modulus ( $314 \pm 50$  kPa) to enable easy surgical handling. Moreover, it had optimal in vitro biocompatibility and was able to separate two different epithelial and connective tissue cell types resembling the ideal in vitro characteristics of a GTR membrane.

### **Acknowledgements:**

This work was carried out with support from China Regenerative Medicine International Limited (CRMI).

### **References**

1. Sam, G. and B.R. Pillai, Evolution of Barrier Membranes in Periodontal Regeneration-"Are the third Generation Membranes really here?". *J Clin Diagn Res*, 2014. **8**(12): p. ZE14-7.
2. Bottino, M.C. and V. Thomas, Membranes for Periodontal Regeneration--A Materials Perspective. *Front Oral Biol*, 2015. **17**: p. 90-100.
3. Kim, H.N., et al., Nanotopography-guided tissue engineering and regenerative medicine. *Advanced drug delivery reviews*, 2013. **65**(4): p. 536-558.
4. Bottino, M.C., et al., Recent advances in the development of GTR/GBR membranes for periodontal regeneration—a materials perspective. *Dental materials*, 2012. **28**(7): p. 703-721.
5. Hutmacher, D., M.B. Hürzeler, and H. Schliephake, A review of material properties of biodegradable and bioresorbable polymers and devices for GTR and GBR applications. *International Journal of Oral & Maxillofacial Implants*, 1996. **11**(5).
6. Needleman, I.G., et al., Guided tissue regeneration for periodontal infra-bony defects. *Cochrane Database Syst Rev*, 2006(2): p. CD001724.
7. Rispoli, L., et al., Surgery Guidelines for Barrier Membranes in Guided Bone Regeneration (GBR). *Journal of Otolaryngology and Rhinology*, 2015. **1**: p. 008.
8. Dimitriou, R., et al., The role of barrier membranes for guided bone regeneration and restoration of large bone defects: current experimental and clinical evidence. *BMC medicine*, 2012. **10**(1): p. 81.
9. Matsuo, A., et al., Clinical application of a custom-made bioresorbable raw particulate hydroxyapatite/poly-L-lactide mesh tray for mandibular reconstruction. *Odontology*, 2010. **98**(1): p. 85-88.
10. Ducheyne, P., et al., Influence of a functional dynamic loading on bone ingrowth into surface pores of orthopedic implants. *Journal of biomedical materials research*, 1977. **11**(6): p. 811-838.
11. Heck, D., et al., The effect of load alteration on the biological and biomechanical performance of a titanium fiber-metal segmental prosthesis. *J Bone Joint Surg Am*, 1986. **68**(1): p. 118-126.
12. Amano, Y., et al., Evaluation of a poly-L-lactic acid membrane and membrane fixing pin for guided tissue regeneration on bone defects in dogs. *Oral Surgery, Oral Medicine, Oral Pathology, Oral Radiology, and Endodontology*, 2004. **97**(2): p. 155-163.
13. O'Brien, F.J., et al., The effect of pore size on cell adhesion in collagen-GAG scaffolds. *Biomaterials*, 2005. **26**(4): p. 433-441.

14. Murphy, C.M., M.G. Haugh, and F.J. O'Brien, The effect of mean pore size on cell attachment, proliferation and migration in collagen–glycosaminoglycan scaffolds for bone tissue engineering. *Biomaterials*, 2010. **31**(3): p. 461-466.
15. Grinnell, F., Cellular adhesiveness and extracellular substrata. *International review of cytology*, 1978. **53**: p. 65-144.
16. Machtei, E.E., et al., Clinical, microbiological, and histological factors which influence the success of regenerative periodontal therapy. *Journal of periodontology*, 1994. **65**(2): p. 154-161.
17. Wikesjö, U., et al., Dynamics of wound healing in periodontal regenerative therapy. *Journal of the California Dental Association*, 1995. **23**(12): p. 30-35.
18. Takata, T., H.L. Wang, and M. Miyauchi, Attachment, proliferation and differentiation of periodontal ligament cells on various guided tissue regeneration membranes. *Journal of periodontal research*, 2001. **36**(5): p. 322-327.
19. Marouf, H.A. and H.M. El-Guindi, Efficacy of high-density versus semipermeable PTFE membranes in an elderly experimental model. *Oral Surgery, Oral Medicine, Oral Pathology, Oral Radiology, and Endodontology*, 2000. **89**(2): p. 164-170.
20. Dimitriou, R., et al., The role of barrier membranes for guided bone regeneration and restoration of large bone defects: current experimental and clinical evidence. *BMC medicine*, 2012. **10**(1): p. 1.
21. Sam, G. and B.R.M. Pillai, Evolution of Barrier Membranes in Periodontal Regeneration- "*Are the third Generation Membranes really here?* *Journal of clinical and diagnostic research: JCDR*, 2014. **8**(12): p. ZE14.
22. Chiara, G., et al., Nanostructured biomaterials for tissue engineered bone tissue reconstruction. *International journal of molecular sciences*, 2012. **13**(1): p. 737-757.
23. Daamen, W.F., et al., Elastin as a biomaterial for tissue engineering. *Biomaterials*, 2007. **28**(30): p. 4378-4398.
24. Burdick, J.A. and G.D. Prestwich, Hyaluronic acid hydrogels for biomedical applications. *Advanced materials*, 2011. **23**(12).
25. Omid, M., A. Yadegari, and L. Tayebi, Wound dressing application of pH-sensitive carbon dots/chitosan hydrogel. *RSC Advances*, 2017. **7**(18): p. 10638-10649.
26. Rasoulianboroujeni, M., et al., From solvent-free microspheres to bioactive gradient scaffolds. *Nanomedicine: Nanotechnology, Biology and Medicine*, 2017. **13**(3): p. 1157-1169.
27. Rasoulianboroujeni, M., S. Pitcher, and L. Tayebi, Fabrication of gradient scaffolds for bone and dental tissue engineering. *Dental Materials*, 2016. **32**: p. e47-e48.
28. Jacobs, P.F., *Rapid prototyping & manufacturing: fundamentals of stereolithography*. 1992: Society of Manufacturing Engineers.
29. Zein, I., et al., Fused deposition modeling of novel scaffold architectures for tissue engineering applications. *Biomaterials*, 2002. **23**(4): p. 1169-1185.
30. Agarwala, M., et al., Direct selective laser sintering of metals. *Rapid Prototyping Journal*, 1995. **1**(1): p. 26-36.
31. Yeong, W.-Y., et al., Rapid prototyping in tissue engineering: challenges and potential. *TRENDS in Biotechnology*, 2004. **22**(12): p. 643-652.
32. Boland, T. and V. Mironov, How to Define Biofabrication? Review of the Book *Biofabrication: Micro-and Nano-Fabrication, Printing, Patterning, and Assemblies*, Edited by Gabor Forgacs and Wei Sun (William Andrew, 2013, 265 Pages). *3D Printing and Additive Manufacturing*, 2014. **1**(1): p. 52-54.
33. Melchels, F.P., et al., Additive manufacturing of tissues and organs. *Progress in Polymer Science*, 2012. **37**(8): p. 1079-1104.
34. Murphy, S.V., A. Skardal, and A. Atala, Evaluation of hydrogels for bio-printing applications. *Journal of Biomedical Materials Research Part A*, 2013. **101**(1): p. 272-284.
35. Skardal, A. and A. Atala, Biomaterials for Integration with 3-D Bioprinting. *Annals of biomedical engineering*, 2014: p. 1-17.
36. Pataky, K., et al., Microdrop Printing of Hydrogel Bioinks into 3D Tissue-Like Geometries. *Advanced Materials*, 2012. **24**(3): p. 391-396.

37. Skardal, A., et al., Bioprinted amniotic fluid-derived stem cells accelerate healing of large skin wounds. *Stem cells translational medicine*, 2012. **1**(11): p. 792-802.
38. Seol, Y.-J., et al., Bioprinting technology and its applications. *European Journal of Cardio-Thoracic Surgery*, 2014: p. ezu148.
39. Binder, K.W., et al., In situ bioprinting of the skin for burns. *Journal of the American College of Surgeons*, 2010. **211**(3): p. 7.
40. Xu, T., et al. Bio-printing of living organized tissues using an inkjet technology. in *NIP & Digital Fabrication Conference*. 2006. Society for Imaging Science and Technology.
41. Xu, T., et al., Complex heterogeneous tissue constructs containing multiple cell types prepared by inkjet printing technology. *Biomaterials*, 2013. **34**(1): p. 130-139.
42. Mironov, V., et al., Organ printing: tissue spheroids as building blocks. *Biomaterials*, 2009. **30**(12): p. 2164-2174.
43. Mironov, V., V. Kasyanov, and R.R. Markwald, Organ printing: from bioprinter to organ biofabrication line. *Current opinion in biotechnology*, 2011. **22**(5): p. 667-673.
44. Hoffman, A.S., Hydrogels for biomedical applications. *Advanced drug delivery reviews*, 2012. **64**: p. 18-23.
45. *Biomaterials for Oral and Dental Tissue Engineering*. 1st Edition ed. 2017: Elsevier-Woodhead Publishing. 562.
46. Shabafrooz, V., et al., The effect of hyaluronic acid on biofunctionality of gelatin–collagen intestine tissue engineering scaffolds. *Journal of Biomedical Materials Research Part A*, 2014. **102**(9): p. 3130-3139.
47. Moharamzadeh, K., et al., Development, optimization and characterization of a full-thickness tissue engineered human oral mucosal model for biological assessment of dental biomaterials. *Journal of Materials Science: Materials in Medicine*, 2008. **19**(4): p. 1793-1801.
48. Rheinwald, J.G. and H. Green, Formation of a keratinizing epithelium in culture by a cloned cell line derived from a teratoma. *Cell*, 1975. **6**(3): p. 317-330.
49. Winter, H., Can the gel point of a cross-linking polymer be detected by the  $G'-G$  "crossover"? *Polymer Engineering & Science*, 1987. **27**(22): p. 1698-1702.
50. Shima Dehghani, M.R., Saeed Heidari Keshel, Hamed GHasemi, Lobat Tayebi, Gelatin Scaffold for Conjunctival Tissue Engineering, in *The 6th Annual Meeting of the Iranian Research Association for Vision And Ophthalmology*. March 3-4, 2016, The Iranian Society of Ophthalmology: Tehran, Iran.
51. Buchanan, F.J., *Degradation rate of bioresorbable materials: Prediction and evaluation*. 2008: Elsevier.
52. Grover, C.N., R.E. Cameron, and S.M. Best, Investigating the morphological, mechanical and degradation properties of scaffolds comprising collagen, gelatin and elastin for use in soft tissue engineering. *Journal of the mechanical behavior of biomedical materials*, 2012. **10**: p. 62-74.